Construction of porous 2D Dy^{3+} metal organic frameworks: Solvent responsive magnetic dynamics under 0 Oe dc field and luminescent sensor for Fe^{3+} ion

Yangyang Gou,[#a] Ming Gao,[#a] Yunlong Wu,[c] Wei Zhou,[a] Jiancheng Feng,[a] Sheng Zhang,[*a] Xiaohong Wang,[*] Bing Yin[*b]

AUTHOR ADDRESS

[a.] *College of Chemistry and Chemical Engineering, Hainan University, Haikou 570228, China*

[b.] *Lab of Theoretical Molecular Magnetism, College of Chemistry and Materials Science, Northwest University, Xi'an, 710127 P. R. China*

[c.] *School of Materials Science & Engineering, Xi'an Polytechnic University, Xi'an 710048, P. R. China*

[#] *These authors contributed equally to the work*

*E-mail: zhangsheng19890501@163.com. (S. Zhang)

*E-mail: wangxiaohong@hainanu.edu.cn

*E-mail: rayinyin@nwu.edu.cn. (B. Yin)

Table S1 Bond Lengths for **1**.

Atom	Atom	Length/Å
Dy1	O24	2.258(2)
Dy1	O22[1]	2.262(2)
Dy1	O2	2.2765(19)
Dy1	O9	2.3056(18)
Dy1	O13	2.3099(18)
Dy1	O5	2.362(2)
Dy1	O25	2.489(2)
Dy2	O14	2.249(2)
Dy2	O16[2]	2.254(2)
Dy2	O10	2.2839(19)
Dy2	O11[3]	2.2882(19)
Dy2	O17[2]	2.3499(18)
Dy2	O26	2.404(2)
Dy2	O1W	2.410(2)
Dy2	O25	2.873(2)
Dy3	O8	2.2515(19)
Dy3	O6[4]	2.270(2)
Dy3	O21	2.277(2)
Dy3	O2W	2.328(2)
Dy3	O1[4]	2.3340(19)
Dy3	O27	2.341(2)
Dy3	O23[4]	2.3723(19)
Dy4	O7	2.2817(18)
Dy4	O12[5]	2.3025(19)
Dy4	O18	2.3101(18)
Dy4	O4[5]	2.367(2)
Dy4	O15	2.368(2)
Dy4	O19[2]	2.454(2)
Dy4	O20[2]	2.4908(18)
Dy4	O3[5]	2.667(2)

[1]+X,3/2-Y,1/2+Z; [2]+X,1/2-Y,1/2+Z; [3]+X,1/2-Y,-1/2+Z; [4]+X,3/2-Y,-1/2+Z; [5]+X,+Y,-1+Z

Table S2 Bond Lengths for **2**.

Atom	Atom	Length/Å
Dy1	O2	2.237(5)
Dy1	O6[1]	2.287(5)
Dy1	O4[2]	2.321(4)

Dy1	O9	2.324(4)
Dy1	O12[3]	2.332(4)
Dy1	O8[4]	2.335(4)
Dy1	O13	2.351(6)
Dy2	O5	2.259(5)
Dy2	O10	2.274(4)
Dy2	O3[2]	2.282(5)
Dy2	O1	2.293(4)
Dy2	O7[5]	2.315(5)
Dy2	O11[4]	2.396(4)
Dy2	O14	2.507(9)
Dy2	O12[4]	2.643(4)

[1]3/2-X,-1/2+Y,3/2-Z; [2]-1/2+X,1/2-Y,-1/2+Z; [3]1-X,-Y,1-Z; [4]1/2+X,1/2-Y,1/2+Z; [5]1-X,1-Y,1-Z

Table S3 Bond Angles for **1**.

Atom	**Atom**	**Atom**	**Angle/°**
O24	Dy1	O22[1]	73.40(10)
O24	Dy1	O2	127.97(8)
O22[1]	Dy1	O2	78.57(10)
O24	Dy1	O9	127.31(9)
O22[1]	Dy1	O9	80.16(9)
O2	Dy1	O9	88.47(8)
O24	Dy1	O13	75.06(8)
O22[1]	Dy1	O13	121.62(10)
O2	Dy1	O13	155.15(8)
O9	Dy1	O13	81.76(7)
O24	Dy1	O5	79.57(9)
O22[1]	Dy1	O5	132.77(9)
O2	Dy1	O5	89.04(9)
O9	Dy1	O5	145.52(7)
O13	Dy1	O5	86.32(8)
O24	Dy1	O25	143.73(9)
O22[1]	Dy1	O25	142.08(9)
O2	Dy1	O25	70.24(9)
O9	Dy1	O25	78.01(7)
O13	Dy1	O25	85.35(8)
O5	Dy1	O25	68.82(8)
O14	Dy2	O16[2]	151.77(9)
O14	Dy2	O10	91.55(8)

O16^{2}	Dy2	O10	99.37(8)
O14	Dy2	O11^{3}	81.13(8)
O16^{2}	Dy2	O11^{3}	77.43(9)
O10	Dy2	O11^{3}	153.20(8)
O14	Dy2	O17^{2}	76.53(8)
O16^{2}	Dy2	O17^{2}	115.89(7)
O10	Dy2	O17^{2}	125.82(8)
O11^{3}	Dy2	O17^{2}	77.68(7)
O14	Dy2	O26	78.39(9)
O16^{2}	Dy2	O26	79.13(9)
O10	Dy2	O26	76.06(9)
O11^{3}	Dy2	O26	77.22(9)
O17^{2}	Dy2	O26	146.77(9)
O14	Dy2	O1W	135.15(8)
O16^{2}	Dy2	O1W	73.07(8)
O10	Dy2	O1W	73.79(8)
O11^{3}	Dy2	O1W	128.57(7)
O17^{2}	Dy2	O1W	78.67(8)
O26	Dy2	O1W	134.44(9)
O14	Dy2	O25	64.69(8)
O16^{2}	Dy2	O25	143.47(8)
O10	Dy2	O25	66.93(7)
O11^{3}	Dy2	O25	129.94(7)
O17^{2}	Dy2	O25	60.14(6)
O26	Dy2	O25	125.55(8)
O1W	Dy2	O25	70.59(7)
O8	Dy3	O6^{4}	157.01(8)
O8	Dy3	O21	77.65(9)
O6^{4}	Dy3	O21	117.18(9)
O8	Dy3	O2W	81.34(8)
O6^{4}	Dy3	O2W	104.02(9)
O21	Dy3	O2W	118.19(10)
O8	Dy3	O1^{4}	89.31(7)
O6^{4}	Dy3	O1^{4}	77.24(8)
O21	Dy3	O1^{4}	79.47(9)
O2W	Dy3	O1^{4}	157.20(9)
O8	Dy3	O27	78.81(9)
O6^{4}	Dy3	O27	80.24(9)
O21	Dy3	O27	147.58(10)

O2W	Dy3	O27	79.52(10)
O1[4]	Dy3	O27	78.27(9)
O8	Dy3	O23[4]	127.40(8)
O6[4]	Dy3	O23[4]	74.58(8)
O21	Dy3	O23[4]	79.38(9)
O2W	Dy3	O23[4]	69.23(8)
O1[4]	Dy3	O23[4]	131.44(7)
O27	Dy3	O23[4]	132.97(9)
O7	Dy4	O12[5]	119.69(7)
O7	Dy4	O18	159.00(7)
O12[5]	Dy4	O18	81.00(8)
O7	Dy4	O4[5]	94.80(9)
O12[5]	Dy4	O4[5]	94.07(9)
O18	Dy4	O4[5]	79.10(8)
O7	Dy4	O15	76.29(8)
O12[5]	Dy4	O15	77.80(9)
O18	Dy4	O15	114.44(8)
O4[5]	Dy4	O15	162.36(9)
O7	Dy4	O19[2]	93.55(7)
O12[5]	Dy4	O19[2]	128.39(7)
O18	Dy4	O19[2]	73.83(7)
O4[5]	Dy4	O19[2]	123.25(7)
O15	Dy4	O19[2]	73.10(8)
O7	Dy4	O20[2]	76.33(7)
O12[5]	Dy4	O20[2]	162.11(8)
O18	Dy4	O20[2]	82.68(7)
O4[5]	Dy4	O20[2]	75.61(8)
O15	Dy4	O20[2]	115.96(8)
O19[2]	Dy4	O20[2]	52.41(6)
O7	Dy4	O3[5]	71.67(7)
O12[5]	Dy4	O3[5]	69.44(7)
O18	Dy4	O3[5]	116.72(7)
O4[5]	Dy4	O3[5]	50.37(7)
O15	Dy4	O3[5]	112.01(8)
O19[2]	Dy4	O3[5]	161.83(7)
O20[2]	Dy4	O3[5]	112.16(7)
Dy1	O25	Dy2	122.04(9)

[1]+X,3/2-Y,1/2+Z; [2]+X,1/2-Y,1/2+Z; [3]+X,1/2-Y,-1/2+Z; [4]+X,3/2-Y,-1/2+Z; [5]+X,+Y,-1+Z; [6]+X,+Y,1+Z

Table S4 Bond Angles for **2**.

Atom	**Atom**	**Atom**	**Angle/°**
O2	Dy1	O6[1]	82.5(2)
O2	Dy1	O4[2]	81.47(18)
O6[1]	Dy1	O4[2]	136.30(17)
O2	Dy1	O9	117.89(18)
O6[1]	Dy1	O9	77.29(18)
O4[2]	Dy1	O9	74.96(18)
O2	Dy1	O12[3]	162.43(16)
O6[1]	Dy1	O12[3]	97.16(17)
O4[2]	Dy1	O12[3]	109.64(15)
O9	Dy1	O12[3]	78.87(15)
O2	Dy1	O8[4]	80.10(18)
O6[1]	Dy1	O8[4]	74.22(19)
O4[2]	Dy1	O8[4]	141.1(2)
O9	Dy1	O8[4]	143.76(18)
O12[3]	Dy1	O8[4]	82.90(16)
O2	Dy1	O13	90.8(3)
O6[1]	Dy1	O13	147.6(2)
O4[2]	Dy1	O13	72.9(2)
O9	Dy1	O13	132.5(2)
O12[3]	Dy1	O13	80.1(2)
O8[4]	Dy1	O13	73.4(2)
O5	Dy2	O10	155.22(18)
O5	Dy2	O3[2]	82.13(19)
O10	Dy2	O3[2]	78.93(19)
O5	Dy2	O1	86.2(2)
O10	Dy2	O1	105.91(18)
O3[2]	Dy2	O1	80.0(2)
O5	Dy2	O7[5]	92.00(19)
O10	Dy2	O7[5]	89.08(17)
O3[2]	Dy2	O7[5]	132.3(2)
O1	Dy2	O7[5]	147.10(19)
O5	Dy2	O11[4]	125.97(17)
O10	Dy2	O11[4]	78.50(16)
O3[2]	Dy2	O11[4]	140.63(17)
O1	Dy2	O11[4]	75.75(19)
O7[5]	Dy2	O11[4]	78.94(19)
O5	Dy2	O14	76.3(3)

O10	Dy2	O14	81.5(3)
O3[2]	Dy2	O14	66.6(3)
O1	Dy2	O14	143.9(3)
O7[5]	Dy2	O14	66.1(3)
O11[4]	Dy2	O14	139.7(3)
O5	Dy2	O12[4]	74.94(16)
O10	Dy2	O12[4]	128.93(15)
O3[2]	Dy2	O12[4]	145.35(18)
O1	Dy2	O12[4]	72.96(15)
O7[5]	Dy2	O12[4]	74.86(16)
O11[4]	Dy2	O12[4]	51.17(13)
O14	Dy2	O12[4]	129.9(3)

[1]3/2-X,-1/2+Y,3/2-Z; [2]-1/2+X,1/2-Y,-1/2+Z; [3]1-X,-Y,1-Z; [4]1/2+X,1/2-Y,1/2+Z; [5]1-X,1-Y,1-Z; [6]3/2-X,1/2+Y,3/2-Z

Table S5 Dy^{III} ion geometry analysis by SHAPE 2.1 software.

Configuration	ABOXIY **1**	
	Dy1	**Dy3**
Heptagon (D_{7h})	29.645	34.850
Hexagonal pyramid (C_{6v})	19.365	19.358
Pentagonal bipyramid (D_{5h})	5.861	7.086
Capped octahedron (C_{3v})	2.294	0.532
Capped trigonal prism (C_{2v})	0.548	1.021
Johnson pentagonal bipyramid J13 (D_{5h})	8.999	10.302
Johnson elongated triangular pyramid J7 J26 (C_{3v})	18.042	18.781
Configuration	ABOXIY **1**	
	Dy2	**Dy4**
Octagon (D_{8h})	29.397	33.269
Heptagonal pyramid (C_{7v})	23.761	24.062
Hexagonal bipyramid (D_{6h})	15.522	7.138
Cube (O_h)	9.681	3.444
Square antiprism (D_{4d})	2.400	6.490
Triangular dodecahedron (D_{2d})	1.424	5.414
Johnson gyrobifastigium J26 (D_{2d})	13.475	11.242
Johnson elongated triangular bipyramid J14 (D_{3h})	25.803	21.051
Biaugmented trigonal prism J50 (C_{2v})	1.320	7.182
Biaugmented trigonal prism (C_{2v})	1.784	6.776
Snub diphenoid J84 (D_{2d})	2.609	9.814

Triakis tetrahedron (T_d)	9.733	3.857
Elongated trigonal bipyramid (D_{3h})	22.491	19.808
Configuration	ABOXIY **2**	
	Dy1	
Heptagon (D_{7h})	33.499	
Hexagonal pyramid (C_{6v})	21.280	
Pentagonal bipyramid (D_{5h})	3.342	
Capped octahedron (C_{3v})	2.039	
Capped trigonal prism (C_{2v})	1.002	
Johnson pentagonal bipyramid J13 (D_{5h})	6.686	
Johnson elongated triangular pyramid J7 J26 (C_{3v})	20.871	
Configuration	ABOXIY **2**	
	Dy2	
Octagon (D_{8h})	29.047	
Heptagonal pyramid (C_{7v})	23.859	
Hexagonal bipyramid (D_{6h})	13.113	
Cube (O_h)	10.968	
Square antiprism (D_{4d})	3.248	
Triangular dodecahedron (D_{2d})	2.243	
Johnson gyrobifastigium J26 (D_{2d})	10.315	
Johnson elongated triangular bipyramid J14 (D_{3h})	26.437	
Biaugmented trigonal prism J50 (C_{2v})	2.133	
Biaugmented trigonal prism (C_{2v})	2.310	
Snub diphenoid J84 (D_{2d})	2.403	
Triakis tetrahedron (T_d)	11.350	
Elongated trigonal bipyramid (D_{3h})	23.695	

S H A P E v2.1 Continuous Shape Measures calculation

(c) 2013 Electronic Structure Group, Universitat de Barcelona

Contact: llunell@ub.edu

1-Dy1 structures

HP-7	1 D7h	Heptagon
HPY-7	2 C6v	Hexagonal pyramid
PBPY-7	3 D5h	Pentagonal bipyramid
COC-7	4 C3v	Capped octahedron
CTPR-7	5 C2v	Capped trigonal prism
JPBPY-7	6 D5h	Johnson pentagonal bipyramid J13

JETPY-7 7 C3v Johnson elongated triangular pyramid J7

Structure [ML7] HP-7 HPY-7 PBPY-7 COC-7 CTPR-7 JPBPY-7 JETPY-7
ABOXIY , 29.645, 19.365, 5.861, 2.294, 0.548, 8.999, 18.042

S H A P E v2.1 Continuous Shape Measures calculation
(c) 2013 Electronic Structure Group, Universitat de Barcelona
Contact: llunell@ub.edu

1-Dy2 structures

OP-8 1 D8h Octagon
HPY-8 2 C7v Heptagonal pyramid
HBPY-8 3 D6h Hexagonal bipyramid
CU-8 4 Oh Cube
SAPR-8 5 D4d Square antiprism
TDD-8 6 D2d Triangular dodecahedron
JGBF-8 7 D2d Johnson gyrobifastigium J26
JETBPY-8 8 D3h Johnson elongated triangular bipyramid J14
JBTPR-8 9 C2v Biaugmented trigonal prism J50
BTPR-8 10 C2v Biaugmented trigonal prism
JSD-8 11 D2d Snub diphenoid J84
TT-8 12 Td Triakis tetrahedron
ETBPY-8 13 D3h Elongated trigonal bipyramid

Structure [ML8] OP-8 HPY-8 HBPY-8 CU-8 SAPR-8 TDD-8 JGBF-8 JETBPY-8 JBTPR-8 BTPR-8 JSD-8 TT-8 ETBPY-8
ABOXIY , 29.397, 23.761, 15.522, 9.681, 2.400, 1.424, 13.475, 25.803, 1.320, 1.784, 2.609, 9.733, 22.491

S H A P E v2.1 Continuous Shape Measures calculation
(c) 2013 Electronic Structure Group, Universitat de Barcelona
Contact: llunell@ub.edu

1-Dy3 structures

HP-7 1 D7h Heptagon
HPY-7 2 C6v Hexagonal pyramid
PBPY-7 3 D5h Pentagonal bipyramid
COC-7 4 C3v Capped octahedron
CTPR-7 5 C2v Capped trigonal prism
JPBPY-7 6 D5h Johnson pentagonal bipyramid J13
JETPY-7 7 C3v Johnson elongated triangular pyramid J7

Structure [ML7] HP-7 HPY-7 PBPY-7 COC-7 CTPR-7 JPBPY-7 JETPY-7
ABOXIY , 34.850, 19.358, 7.086, 0.532, 1.021, 10.302, 18.781

S H A P E v2.1 Continuous Shape Measures calculation
(c) 2013 Electronic Structure Group, Universitat de Barcelona
Contact: llunell@ub.edu

1-Dy4 structures

OP-8 1 D8h Octagon
HPY-8 2 C7v Heptagonal pyramid
HBPY-8 3 D6h Hexagonal bipyramid
CU-8 4 Oh Cube
SAPR-8 5 D4d Square antiprism
TDD-8 6 D2d Triangular dodecahedron
JGBF-8 7 D2d Johnson gyrobifastigium J26
JETBPY-8 8 D3h Johnson elongated triangular bipyramid J14
JBTPR-8 9 C2v Biaugmented trigonal prism J50
BTPR-8 10 C2v Biaugmented trigonal prism
JSD-8 11 D2d Snub diphenoid J84
TT-8 12 Td Triakis tetrahedron
ETBPY-8 13 D3h Elongated trigonal bipyramid

Structure [ML8] OP-8 HPY-8 HBPY-8 CU-8 SAPR-8 TDD-8 JGBF-8 JETBPY-8 JBTPR-8 BTPR-8 JSD-8 TT-8 ETBPY-8
ABOXIY , 33.269, 24.062, 7.138, 3.444, 6.490, 5.414, 11.242, 21.051, 7.182, 6.776, 9.814, 3.857, 19.808

S H A P E v2.1 Continuous Shape Measures calculation
(c) 2013 Electronic Structure Group, Universitat de Barcelona
Contact: llunell@ub.edu

2-Dy1 structures

HP-7 1 D7h Heptagon
HPY-7 2 C6v Hexagonal pyramid
PBPY-7 3 D5h Pentagonal bipyramid
COC-7 4 C3v Capped octahedron
CTPR-7 5 C2v Capped trigonal prism
JPBPY-7 6 D5h Johnson pentagonal bipyramid J13
JETPY-7 7 C3v Johnson elongated triangular pyramid J7

Structure [ML7] HP-7 HPY-7 PBPY-7 COC-7 CTPR-7 JPBPY-7 JETPY-7

ABOXIY , 33.499, 21.280, 3.342, 2.039, 1.002, 6.686, 20.871

S H A P E v2.1 Continuous Shape Measures calculation
(c) 2013 Electronic Structure Group, Universitat de Barcelona
Contact: llunell@ub.edu

2-Dy2 structures

OP-8	1 D8h	Octagon
HPY-8	2 C7v	Heptagonal pyramid
HBPY-8	3 D6h	Hexagonal bipyramid
CU-8	4 Oh	Cube
SAPR-8	5 D4d	Square antiprism
TDD-8	6 D2d	Triangular dodecahedron
JGBF-8	7 D2d	Johnson gyrobifastigium J26
JETBPY-8	8 D3h	Johnson elongated triangular bipyramid J14
JBTPR-8	9 C2v	Biaugmented trigonal prism J50
BTPR-8	10 C2v	Biaugmented trigonal prism
JSD-8	11 D2d	Snub diphenoid J84
TT-8	12 Td	Triakis tetrahedron
ETBPY-8	13 D3h	Elongated trigonal bipyramid

Structure [ML8] OP-8 HPY-8 HBPY-8 CU-8 SAPR-8 TDD-8 JGBF-8 JETBPY-8 JBTPR-8 BTPR-8 JSD-8 TT-8 ETBPY-8

ABOXIY , 29.047, 23.859, 13.113, 10.968, 3.248, 2.243, 10.315, 26.437, 2.133, 2.310, 2.403, 11.350, 23.695

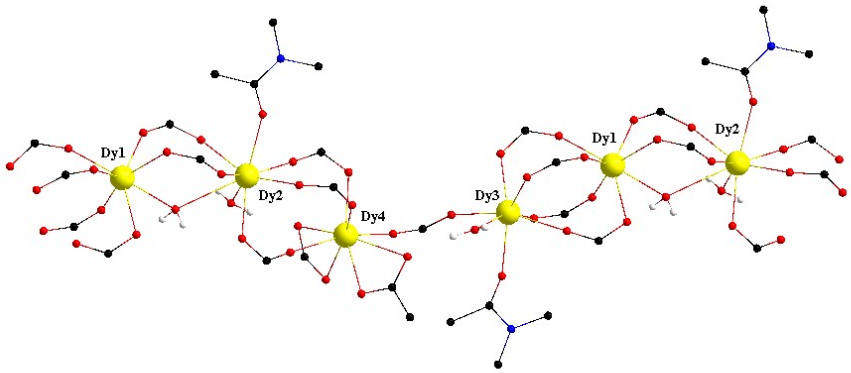

Figure S1. The connection modes between metal ions in compound **1**. Hydrogen, H; blue, N; yellow, Dy; red, O; Black, C.

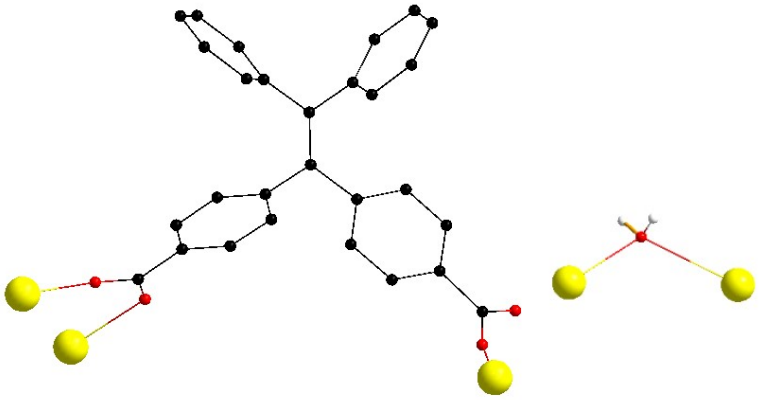

(a) (b)

Figure S2. The coordination modes of ligand and water molecule in compound **1**. Hydrogen, H; yellow, Dy; red, O; Black, C.

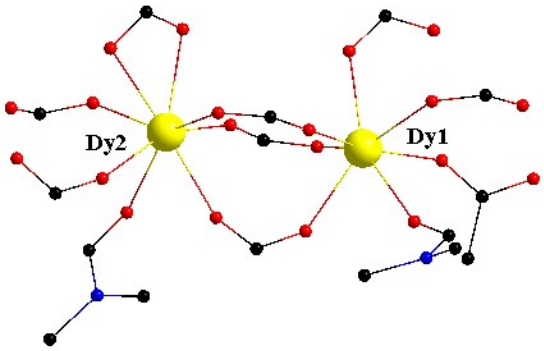

Figure S3. The connection modes between metal ions in compound **2**. Blue, N; yellow, Dy; red, O; Black, C.

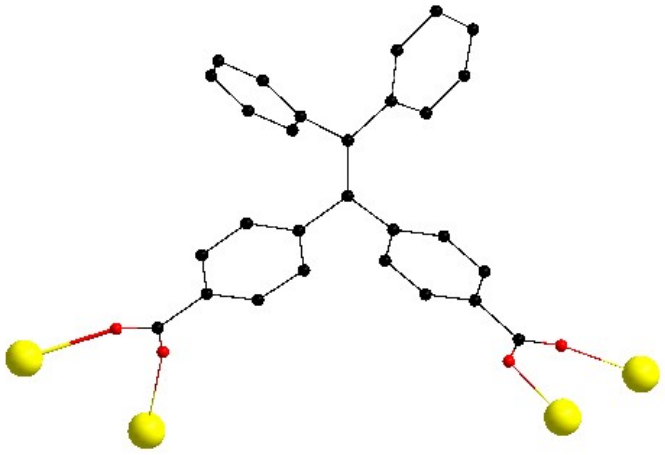

Figure S4. The connection modes between metal ions in compound **2**. Yellow, Dy; red, O; Black, C.

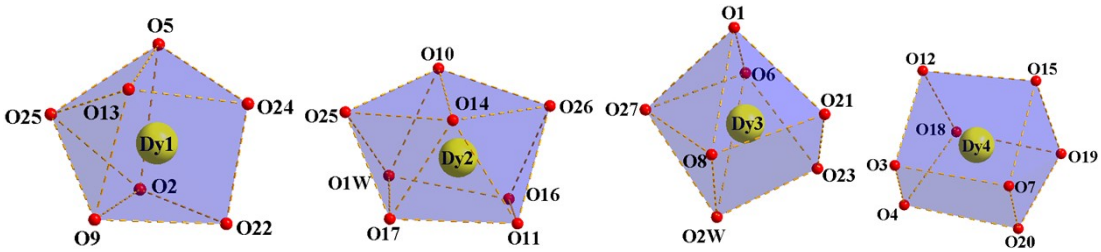

Figure S5. Local coordination geometries of the Dy^{3+} ions for **1.** Yellow, Dy; red, O.

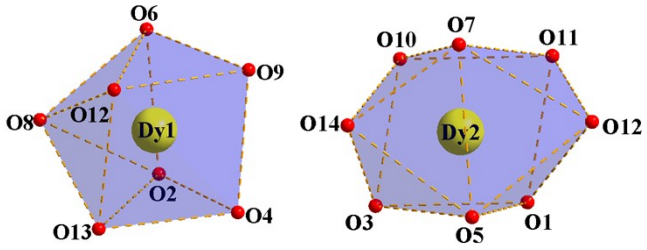

Figure S6. Local coordination geometries of the Dy^{3+} ions for **2.** Yellow, Dy; red, O.

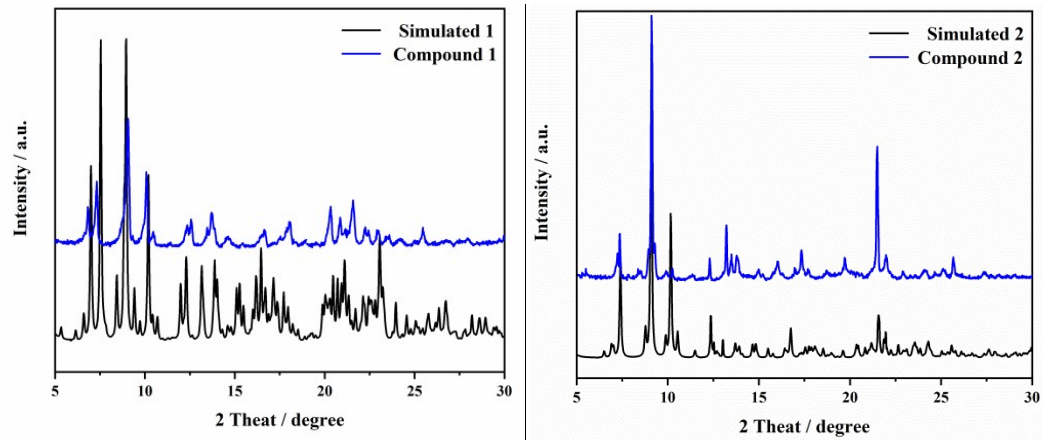

(a) (b)

Figure S7. PXRD curves of **1** (a) and **2** (b).

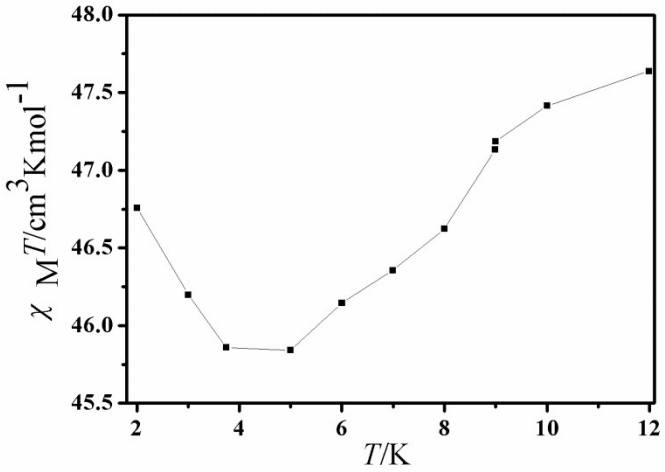

Figure S8. Temperature dependence of $\chi_M T$ measured at 1 KOe for **1**, respectively.

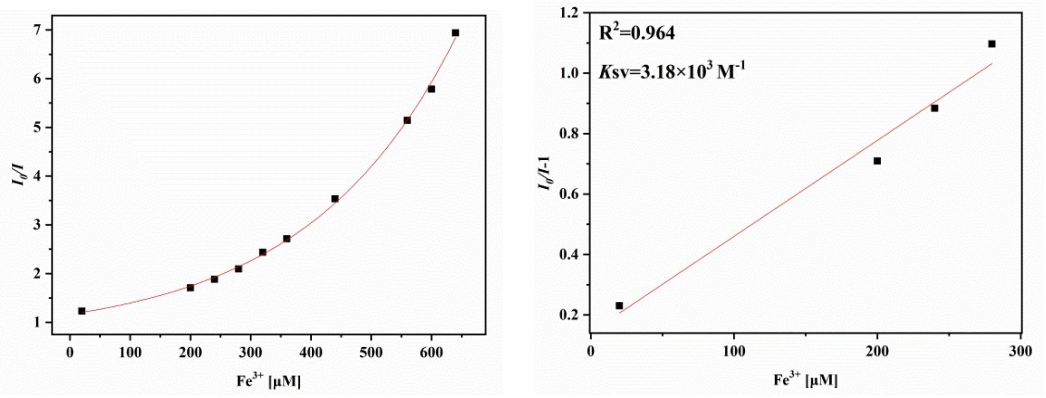

(a) (b)

Figure S9. (a) The SV spectrum of Fe^{3+} for compound **1**; (b) Stern-Volmer fitting curve for compound **1**.

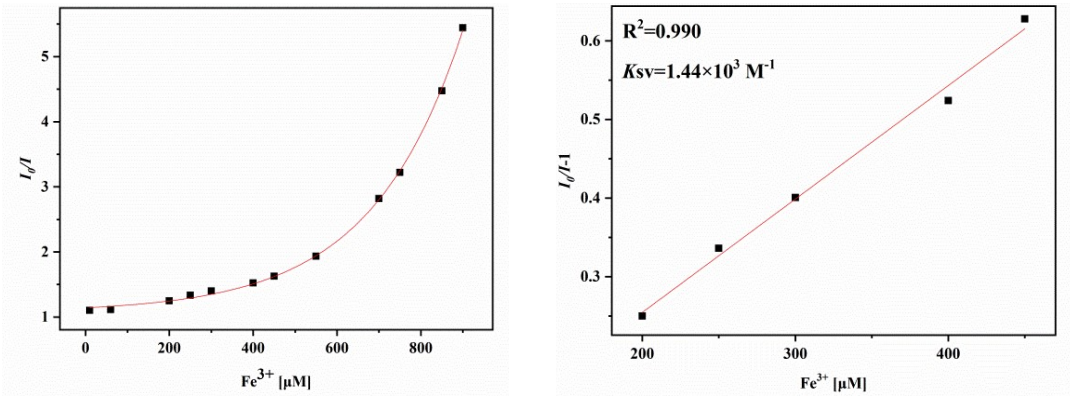

(a) (b)

Figure S10. (a) The SV spectrum of Fe^{III} for compound **2** (a); (b) Stern-Volmer fitting curve for compound **2**.

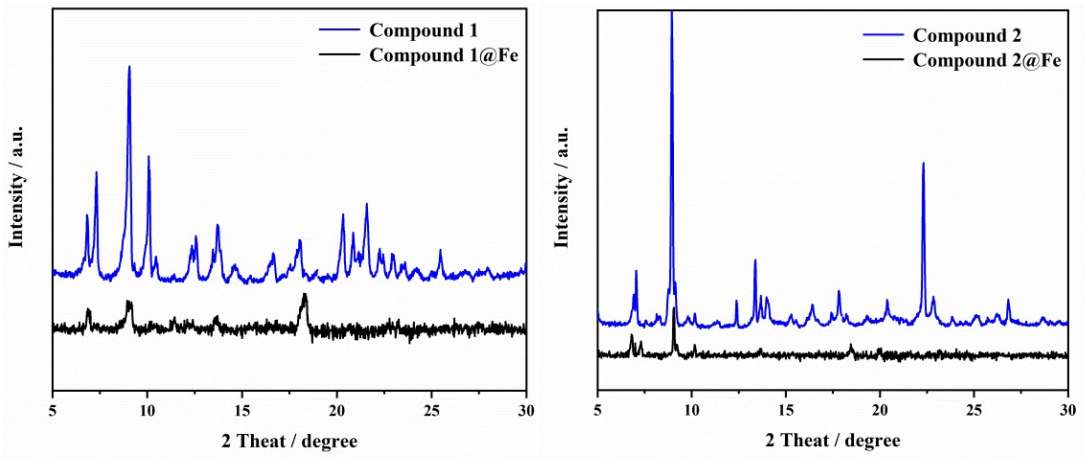

(a) (b)

Figure S11. The PXRD patterns for compounds **1** (a) and **2** (b) after fluorescent detection.

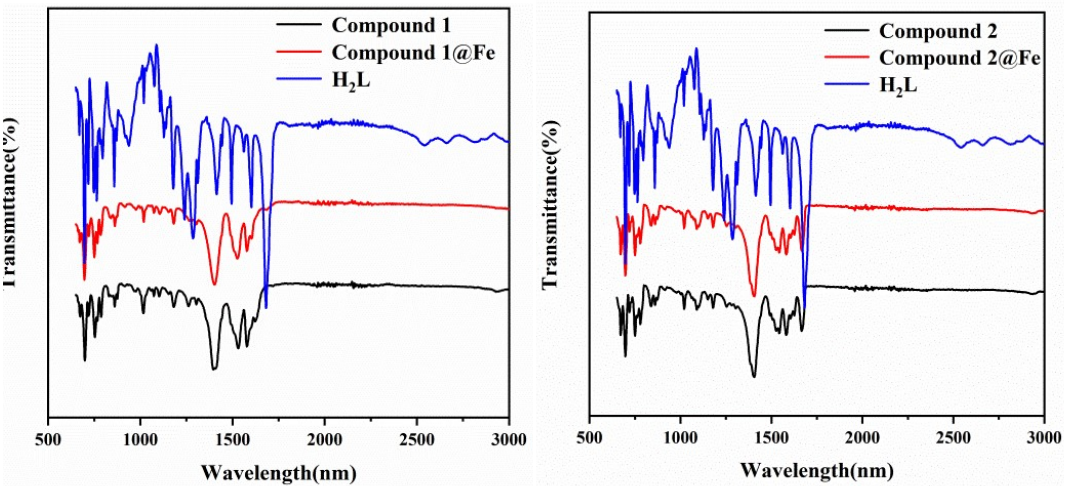

(a) (b)

Figure S12. The FT-IR patterns for compounds **1** (a) and **2** (b) after fluorescent detection.

Computational details

Multiconfigurational *ab initio* calculations, including spin-orbit coupling (SOC), were performed on selected systems. This type of calculation includes two steps:[1] 1) a set of spin eigenstates, are obtained by the state-averaged (SA) CASSCF method;[2] 2) the Kramers doublets (KDs) are obtained by state interaction which is the diagonalization of the SOC matrix in the space spanned by the spin eigenstates from the first step. In the CASSCF step, the active space consisted of 9 electrons in 7 orbitals and all the spin eigenstates of 21 sextets were included. The scalar relativistic effect is accounted via DKH2 Hamiltonian. The second step was performed via the RASSI-SO module[3] with the SOC integrals from the AMFI method.[4] The ANO-RCC type basis set,[5,6] including VTZP for Dy, VDZ for C and H as well as VDZP for other atoms, was used. All the calculations were carried out with the MOLCAS@UU, a freely academic version of MOLCAS 8.0 code.[7] The SINGLE ANISO module[8,9] was used to obtain the g-tensors.

Table S6 Calculated energy levels (cm^{-1}), $\boldsymbol{g}$ (g_x, g_y, g_z) tensors of the lowest eight KDs of individual Dy^{III} fragments of compounds **1** and **2** using CASSCF/RASSI-SO with MOLCAS 8.2.

Compound **1**								
Str1_modelA	KD_0	KD_1	KD_2	KD_3	KD_4	KD_5	KD_6	KD_7
g_X	1.017E-01	8.020E+00	1.782E+00	3.384E-01	1.662E+00	5.322E-01	1.037E-01	1.621E-02

g_Y	2.097E-01	2.605E+00	2.820E+00	2.719E+00	2.325E+00	7.919E-01	2.244E-01	1.133E-01
g_Z	1.955E+01	1.080E+01	1.090E+01	1.345E+01	1.386E+01	1.759E+01	1.941E+01	1.961E+01
E (cm^{-1})	0.000E+00	1.660E+02	2.090E+02	2.476E+02	2.856E+02	3.443E+02	4.344E+02	4.971E+02
Str1_modelB	KD0	KD1	KD2	KD3	KD4	KD5	KD6	KD7
g_X	1.607E-02	4.817E-01	8.596E-01	5.715E+00	2.253E+00	1.705E+00	1.744E-01	3.909E-02
g_Y	2.456E-02	1.235E+00	1.668E+00	9.418E-01	3.739E+00	2.367E+00	2.256E-01	8.968E-02
g_Z	1.964E+01	1.829E+01	1.402E+01	1.016E+01	1.045E+01	1.241E+01	1.747E+01	1.932E+01
E (cm^{-1})	0.000E+00	7.620E+01	1.100E+02	1.456E+02	1.695E+02	2.227E+02	3.639E+02	4.719E+02
Str1_modelC	KD0	KD1	KD2	KD3	KD4	KD5	KD6	KD7
g_X	2.510E-01	5.230E-01	1.340E+00	6.998E+00	4.116E-01	5.117E-01	5.197E-02	1.969E-01
g_Y	7.958E-01	1.316E+00	2.931E+00	2.498E+00	4.122E+00	3.810E+00	1.116E+00	7.561E-01
g_Z	1.810E+01	1.549E+01	1.280E+01	8.273E+00	1.046E+01	1.467E+01	1.818E+01	1.872E+01
E (cm^{-1})	0.000E+00	3.876E+01	9.869E+01	1.751E+02	2.423E+02	2.973E+02	3.478E+02	3.730E+02
Str1_modelD	KD0	KD1	KD2	KD3	KD4	KD5	KD6	KD7
g_X	5.741E-01	6.027E-01	1.500E+00	4.020E+00	9.448E-02	2.338E+00	2.244E+00	4.424E-01
g_Y	1.526E+00	1.866E+00	3.662E+00	5.848E+00	5.499E-01	3.626E+00	3.692E+00	1.210E+00
g_Z	1.800E+01	1.344E+01	1.145E+01	1.107E+01	1.386E+01	1.173E+01	1.193E+01	1.658E+01
E (cm^{-1})	0.000E+00	4.675E+01	8.242E+01	1.523E+02	2.379E+02	3.179E+02	3.761E+02	4.414E+02
Str2_modelA	KD0	KD1	KD2	KD3	KD4	KD5	KD6	KD7
g_X	2.642E-01	1.717E-01	1.852E+00	2.417E+00	2.613E+00	1.745E-01	4.092E-02	3.550E-02
g_Y	4.375E-01	3.367E-01	2.425E+00	5.443E+00	3.909E+00	3.353E-01	2.018E-01	9.605E-02
g_Z	1.884E+01	1.899E+01	1.378E+01	1.073E+01	1.263E+01	1.913E+01	1.734E+01	1.890E+01
E (cm^{-1})	0.000E+00	4.284E+01	9.527E+01	1.674E+02	2.052E+02	2.987E+02	3.618E+02	4.189E+02
Str2_modelB	KD0	KD1	KD2	KD3	KD4	KD5	KD6	KD7
g_X	7.053E-03	6.621E-02	2.889E+00	7.547E+00	1.751E+00	2.605E+00	8.743E-02	1.684E-01
g_Y	1.847E-01	2.624E-01	3.384E+00	2.579E+00	4.071E+00	4.490E+00	6.160E-01	7.059E-01
g_Z	1.907E+01	1.894E+01	1.368E+01	8.176E+00	9.834E+00	1.347E+01	1.622E+01	1.823E+01
E (cm^{-1})	0.000E+00	2.147E+01	9.395E+01	1.369E+02	2.032E+02	2.483E+02	3.150E+02	3.566E+02

Table S7 Standard deviation (σ) caculation for the detecation of $Fe^{3+}$for compound **1**.

Test	fluorescence intensity (a.u.)
1	141141
2	141253
3	141094
average	141163
standard deviation	81.68

Table S8 Standard deviation (σ) caculation for the detecation of $Fe^{3+}$for compound **2**.

Test	fluorescence intensity (a.u.)
1	67059

2	67141
3	67097
average	67099
standard deviation	41.03

Table S9 Comparison of inductive capability of Fe^{3+} for compounds **1, 2** and other luminescence MOFs

Materials	$K_{SV}(M^{-1})$	Detection limition (ppb)	Solvent	Reference
Compound **1**	3.18×10^3	4.51×10^6	water	This work
Compound **2**	1.44×10^3	6.90×10^6	water	This work
$[Zn_2(4,4'\text{-nba})_2(1,4\text{-bib})_2]_n$	2.54×10^4	1.29×10^6	water	[10]
$[Zn(L)_{0.5}(MIP)]_n$	6.50×10^3	2.20×10^5	water	[11]
$\{[Zn_2(L)(TBIP)_{1.5}(OH)]\cdot H_2O\}_n$	1.13×10^4	1.30×10^5	water	[12]
$\{[Zn_3(bpg)_{1.5}(azdc)_3]\cdot(DMF)_{5.9}\cdot(H_2O)_{1.05}\}_n$	4.70×10^4	1.00×10^6	water	[13]
$\{[Zn_3(mtrb)_3(btc)_2]\cdot3H_2O\}_n$	3.19×10^4	2.00×10^5	water	[14]
$[Zn(L)_{0.5}(MIP)]_n$	2.25×10^4	5.40×10^5	water	[14]
$Zn(L)(DBT)_n$	1.29×10^4	6.50×10^5	water	[14]
$[Eu(L)(H_2O)_3]_n$	9.60×10^5	4.50×10^3	DMF	[15]
$TbDTTA[Tb(L)(H_2O)_3]_n$	8.39×10^4	1.79×10^6	water	[15]
$[Cd_{1.5}(L)_2(bpy)(NO_3)]\cdot2DMF\cdot2H_2O$	6.02×10^4	1.02×10^5	DMF	[15]
$[Eu_{0.5}Tb_{0.5}(L)(H_2O)_3]_n$	4.20×10^5	6.40×10^4	DMF	[15]
$[Zn(FDC)_2(H_2O)_2]_n$	3.93×10^4	9.00×10^5	water	[16]
$\{[Cd(L)\text{- }(BPDC)]\cdot2H_2O\}_n$	1.68×10^4	1.76×10^6	water	[17]
$[Zn(L)_2]_n$	3.63×10^4	2.21×10^6	water	[18]
$\{[Cd(L)\ (SDBA)](H_2O)].0.5H_2O\}_n$	3.59×10^4	7.14×10^6	water	[18]
EuDTTA	3.63×10^4	4.14×10^6	water	[19]
$\{[Zn_4(\mu_3\text{-}OH)_2(BTC)_2(BBI4PY)_2].10H_2O\}_n$	3.93×10^4	9.00×10^5	water	[20]
$[Zn_2(L)_2(TPA)]\cdot2H_2O$	6.40×10^3	3.84×10^6	water	[21]
$Eu_{0.24}Tb_{0.76}$-BIM-COOH-PLA	1.27×10^4	4.47×10^6	water	[22]
$\{[Eu_2(ppda)_2(npdc)(H_2O)]H_2O\}_n$	1.64×10^5	1.66×10^7	water	[23]
PAF-5CF	1.18×10^3	3.80×10^7	ethanol	[24]
$\{[Zn_2(\mu_4\text{-L})(\mu_3\text{-bta})(3H_2O)]\cdot H_2O\}_n$	1.06×10^4	1.10×10^8	water	[25]
534-MOF-Tb	5.51×10^3	1.30×10^8	water	[26]
$[Zn(modbc)_2]$(Zn-CP)	7.20×10^3	5.70×10^8	water	[27]

References

[1] J. Luzón and R. Sessoli, Lanthanides in molecular magnetism: so fascinating, so challenging. *Dalton Trans.* 2012, **41**, 13556-13567.

[2] B. O. Roos, P. R. Taylor and P. E. M. Siegbahn, A complete active space SCF method (CASSCF) using a density matrix formulated super-CI approach, *Chem. Phys*., 1980, **48**, 157-173.

[3] P. Malmqvist, B. O. Roos and B. Schimmelpfennig, The restricted active space (RAS) state interaction approach with spin-orbit coupling, *Chem. Phys. Lett.,* 2002, **357**, 230-240.

[4] B. A. Hess, C. M. Marian, U. Wahlgren and O. Gropen, A mean-field spin-orbit method applicable to correlated wavefunctions, *Chem. Phys. Lett.,* 1996, **251**, 365-371.

[5] B. O. Roos, R. Lindh, P. Malmqvist, V. Veryazov and P. Widmark, Main group atoms and dimers studied with a new relativistic ANO basis set, *J. Phys. Chem. A*., 2004, **108**, 2851–2858.

[6] B. O. Roos, R. Lindh, P. Malmqvist, V. Veryazov, P. Widmark and A. C. Borin, New relativistic atomic natural orbital basis sets for lanthanide atoms with applications to the Ce diatom and LuF_3, *J. Phys. Chem. A*., 2008, **112**, 11431–11435.

[7] F. Aquilante, J. Autschbach, R. K. Carlson, L. F. Chibotaru, M. G. Delcey, L. De. Vico, I. F. Galván, N. Ferré, L. M. Frutos, L. Gagliardi, M. Garavelli, A. Giussani, C. E. Hoyer, G. Li. Manni, H. Lischka, D. X. Ma, P. Malmqvist, T. Müller, A. Nenov, M. Olivucci, T. B. Pedersen, D. L. Peng, F. Plasser, B. Pritchard, M. Reiher, I. Rivalta, I. Schapiro, M. J. Segarra, M. Stenrup, D. G. Truhlar, L. Ungur, A. Valentini, S. Vancoillie, V. Veryazov, V. P. Vysotskiy, O. Weingart, F. Zapata and R. Lindh, Molcas 8: New capabilities for multiconfigurational quantum chemical calculations across the periodic table, *J. Comput. Chem*., 2016, **37**, 506–541.

[8] L. F. Chibotaru and L. Ungur, Ab initio calculation of anisotropic magnetic properties of complexes. I. Unique definition of pseudospin Hamiltonians and their derivation, *J. Chem. Phys*., 2012, **137**, 064112.

[9] L. F. Chibotaru, *Ab initio* methodology for pseudospin Hamiltonians of anisotropic magnetic complexes, *Adv. Chem. Phys.,* 2013, **153**, 397–519.

[10] R. Goswami, S.C. Mandal, B. Pathak and S. Neogi, Guest-induced ultrasensitive detection of multiple toxic organics and Fe^{3+} ions in a strategically designed and

regenerative smart fluorescent metal–organic framework, *ACS Appl. Mater. Interfaces.,* 2019, **11** ,9042-9053.

[11] Y. Q. Zhang, V. A. Blatov, T. R. Zheng, C. H. Yang, L. L. Qian, K. Li, B. L. Li and B. Wu, A luminescent zinc (II) coordination polymer with unusual (3, 4, 4)-coordinated self-catenated 3D network for selective detection of nitroaromatics and ferric and chromate ions: a versatile luminescent sensor, *Dalton Trans*., 2018, **47**, 6189-6198.

[12] M. Singh, S. Senthilkumar, S. Rajput and S. Neogi, Pore-functionalized and hydrolytically robust Cd (II)-metal–organic framework for highly selective, multicyclic CO_2 adsorption and fast-responsive luminescent monitoring of Fe (III) and Cr (VI) ions with notable sensitivity and reusability, *Inorg. Chem.*, 2020, **59**, 3012-3025.

[13] Z. H. Wang, X. Z. Wang, X.Y. Lai, Q. Hou, J. X. Ma, J. H. Li, K.Yue and Q. F. Yang, Three new coordination polymers based on a fluorene derivative ligand for the highly luminescent sensitive detection of Fe^{3+}, *J. Mol. Struct.*, 2020, **1202** ,127341-127350.

[14] H. Zhu, L. S. Fu, D. Liu, Y. H. Li and G. Y. Dong, Three water-stable luminescent Zn (II) coordination polymers for highly sensitive and selective sensing of acetylacetone and Fe^{3+} ions, *J. Solid State Chem*., 2020, **286**, 121265-121274.

[15] X. F. Cheng, J. S. Hu, J. X. Li, M and D. Zhang, Tunable emission and selective luminescence sensing for nitro-pollutants and metal ions based on bifunctional lanthanide metal-organic frameworks, *J. Lumin*., 2020, **221**, 117100-117110.

[16] S. Khan, P. Das and S. K. Mandal, Design and construction of a luminescent and highly stable 3D metal–organic framework with a $[Zn_4(\mu_3\text{-}OH)_2]^{6+}$ core, *Inorg. Chem*., 2020, **59**, 4588-4600.

[17] T. Y. Xu, J. M. Li, Y. H. Han, A. R. Wang, K. H. He and Z. F. Shi, A new 3D four-fold interpenetrated dia-like luminescent Zn (II)-based metal–organic framework: The sensitive detection of Fe^{3+}, $Cr_2O_7^{2-}$, and CrO_4^{2-} in water, and nitrobenzene in ethanol, *New J. Chem*., 2020, **44**, 4011-4022.

[18] S. G. Chen, Z. Z. Shi, L. Qin, H. L. Jia, H and G. Zheng, Two new luminescent

Cd (II)-MOFs as bi-functional chemosensors for detection of cations Fe^{3+}, anions CrO_4^{2-} and $Cr_2O_7^{2-}$ in aqueous solution, *Cryst. Growth Des*., 2017, **17**, 67-72.

[19] Y. Zhang, L. Wu and M. Feng, Assembly of two-dimension LMOF materials with excellent detection of Fe^{3+} ion in water based on overlap mechanism, *J. Solid State Chem*., 2020, **294**, 121868-121874.

[20] S. Khan, P. Das and S. K. Mandal, Design and construction of a luminescent and highly stable 3D metal–organic framework with a $[Zn_4(\mu_3\text{-}OH)_2]^{6+}$ core, *Inorg. Chem*., 2020, **59**, 4588-4600.

[21] X. Y. Guo, Z. P. Dong, F. Zhao, Z. L. Liu and Y. Q. Wang, Zinc (II)–organic framework as a multi-responsive photoluminescence sensor for efficient and recyclable detection of pesticide 2, 6-dichloro-4-nitroaniline, Fe (III) and Cr (VI), *New J. Chem*., 2019, **43**, 2353-2361.

[22] P. Jia, Z. H. Wang, Y. F. Zhang, D. Zhang, W. C. Gao, Y. Su, Y. B. Li and C. L. Yang, Selective sensing of Fe^{3+} ions in aqueous solution by a biodegradable platform based lanthanide metal organic framework, *Spectrochim. Acta A.,* 2020, **230**, 118084-118092.

[23] C. L. Li, F. Zhang, X. Li, G.W. Zhang and Y. Y. Yang, A luminescent Ln-MOF thin film for highly selective detection of nitroimidazoles in aqueous solutions based on inner filter effect, *J. Lumin*., 2019, 205, 23-29.

[24] T. T. Ma, X. Zhao, Y. Matsuo, J. Song, R. Zhao, M. Faheem, M. Chen, Y. F. Zhang, Y. Y. Tian and G. S. Zhu, Fluorescein-based fluorescent porous aromatic framework for Fe^{3+} detection with high sensitivity, *J. Mater. Chem. C.,* 2019, **7**, 2327-2332.

[25] Y. X. Yang, S. Y. Xia, H. X. Zhang, H. H. Niu, W. J. Dong and X. X. Wu, *J. Solid State Chem.,* 2020, **284**, 121180.

[26 M. Chen, W. M. Xu, J.Y. Tian, H. Cui, J. X. Zhang, C. S. Liu and M. Du, A terbium (III) lanthanide–organic framework as a platform for a recyclable multi-responsive luminescent sensor, *J. Mater. Chem. C.,* 2017, **5**, 2015-2021.

[27] Y. D. Wu, D.Y. Liu, M. H. Lin and J. Qian, Zinc (ii)-based coordination polymer encapsulated Tb^{3+} as a multi-responsive luminescent sensor for Ru^{3+}, Fe^{3}+, CrO_4^{2-},

$Cr_2O_7^{2-}$ and MnO^{4-}, *RSC Adv.,* 2020, **10**, 6022-6029.